Chapter 4

Solubility and *in Vitro* Drug Permeation Behaviour of Ethenzamide Cocrystals Regulated in Physiological pH Environments

4.1 Abstract

This chapter reports the synthesis of four different cocrystals consisting of a BCS class-II drug ethenzamide with gentisic acid; γ-resorcylic acid; protocatechuic acid; α-resorcylic acid as coformers. Cocrystals are characterized by using different analytical techniques and subjected to determine the solubility and membrane diffusion behavior at different physiological pH environments. These improved properties are correlated with different non-covalent interactions developed from drug···coformer and solute···solvent interactions by determining their single crystal X-ray structures. The change in lipophilic nature manifested by conformational adjustment of the parent drug in cocrystals has established a linked for the attributed enhanced properties and emphasized herein. Further, this study also demonstrates the *trade-off* nature between solubility and diffusivity which is crucial for determining drug efficacy.

4.2 Introduction

Pharmacokinetics has vital significance in the context of drug efficiency, as it relates to the rate, extent of drug release and absorption, the dosage, time course, and the mechanisms of excretion. Over 80% of drugs are in solid formulations and administered orally, which are absorbed via passive diffusion through the gastrointestinal tract [1,2]. Thus it is essential to have desired solubility and membrane permeation profile of a drug for its better bioavailability and efficacy. These factors are closely related to drug structure and largely on intermolecular interactions between drug···excipient and solute···solvent. Additionally, to facilitate drug permeation through biological membranes, it is essential that orally administered drugs must possess certain lipophilicity, which assists to interact adequately with the media and solutes [3,4]. On the other hand, the newly emerging cocrystal is an enabling technology used in new or existing drug delivery systems for product improvement synergistically by changing conformation and intermolecular interactions [5–9]. Therefore, designing a

pharmaceutical cocrystal with high solubility and permeability, which are desired for better oral absorption, has become a natural practice. Essentially coformers/excipients play important roles in changing the lipophilic nature of the drug. It is reported that higher solubility of a cocrystal can be achieved by picking a highly soluble coformer [7]. However, the adjustment of drug/coformer conformation may lead to the best interactions model for the drug; as a result, the physicochemical and mechanical properties are not identical. So, cocrystallization strategy provides a unique aspect to alter drug conformation by developing pharmaceutical cocrystals especially drug ···drug cocrystals. The role of drug···coformer interactions while elucidating the enhancement in solubility of diuretic, hydrochlorothiazide via cocrystallization has been emphasized recently [10]. In Chapter 3, we have demonstrated membrane permeation behaviour and interlinks between solubility/permeability with the supramolecular structure of cocrystals in stoichiometry cocrystals at physiological pH environment [11]. The enhanced solubility and improved diffusivity in different pH conditions for multicomponent solid comprising of an antibacterial (norfloxacin) and an antimicrobial (sulfathiazole) is also reported [12]. Considering indomethacin-saccharin cocrystal, Velega et al. emphasized the cocrystals having higher aqueous solubility can lead to improvement *in-vivo* bioavailability [13]. Though, there are several reports available that talk about the property amendment of drug molecules through cocrystallization, yet it demands extensive understanding as only a few are approved and available in the market. As per the US Food and Drug Administration (FDA) classification of APIs based on solubility and permeability in the "Biopharmaceutics Classification Systems (BCS)", about 30% of commercially available drugs fall in BCS class II drugs, having limited pharmacokinetic properties, that seek treatment to improve drug properties [14].

The results deliberated in this chapter will highlight the synthesis of four cocrystals for improved properties of BCS class-II drug ethanzemide (ZMD) as it has extremely low aqueous solubility (0.034 mg/mL) and poor permeation behaviour [15]. Aqueous solubility and membrane permeation at different pH buffers (pH at 1.2, and 7.4) are determined for these cocrystals and demonstrated how intermolecular interactions between drug···coformer; solute···solvent can play a pivotal role in changing solubility and membrane permeation behaviour that predicts the efficacy of the drug. The

improvements of properties of the drug-mediated by various supramolecular interactions and change in drug conformation have been investigated in these cocrystals. This study accounts how alteration of the lipophilic behaviour by tuning weak intermolecular interactions, and conformational adjustment of the drug contributes towards the modification of drug solubility and permeation profile. Phase stability at different pH buffers and trade-off nature between solubility and permeability are also examined. Finally, it sought a way out of combination with improved drugs properties in pharmaceutical developments.

4.3 Results and Discussion

4.3.1 Synthesis

Ethenzamide is a non-steroidal anti-inflammatory drug (NSAID), which can act as an antioxidant free radical scavenger. However, different oxidants can impair the major inhibiting system of NSAIDs, primarily through anti-inflammatory mechanism [16]. Hence, drug formulation which comprises antioxidant usually offers a solution to improve the activity of NSAIDs. In view of that, we prepared cocrystals of ZMD with coformer possessing antioxidant activity such as 2,5-dihydroxybenzoic acid (2,5-DHBA, gentisic acid, antiparkinson activity, an antioxidant excipients, antirheumatic excipients), 2,6-dihydroxybenzoic acid (2,6-DHBA, γ-resorcylic acid, an antioxidant), 3,4-dihydroxybenzoic acid (3,4-DHBA, protocatechuic acid, an antioxidant and anti-inflammatory) and 3,5-dihydroxybenzoic acid (3,5-DHBA, α-resorcylic acid, an antioxidant) (Scheme 4.1). Four stoichiometric cocrystals were isolated from liquid assisted mechanochemical grinding followed by slow evaporation of solvents and characterized by FT-IR, DSC, TGA, PXRD and SCXRD (details are in experimental section 4.5). Remaining two DHBA isomers in this series, i.e. 2, 4- and 2, 3-DHBA did not afford pure cocrystal materials and deferred to include in this study.

It appears that study on ZMD cocrystals took a rapid pace at the time of our report presented in this chapter [15]. Literature reveals that SCXRD of three polymorphic phases of ZMD·2,5-DHBAcocrystal, ZMD·3,5-DHBA, ZMD·3,5-DHBA·2H_2O, ZMD·2,4-DHBA has been reported [17–19]. Therefore the scope of the study is to examine the solubility and *in-vitro* drug membrane permeation behaviour of

these cocrystals regulated at various physiological pH environments which essentially dictates the bioavailability of that drug.

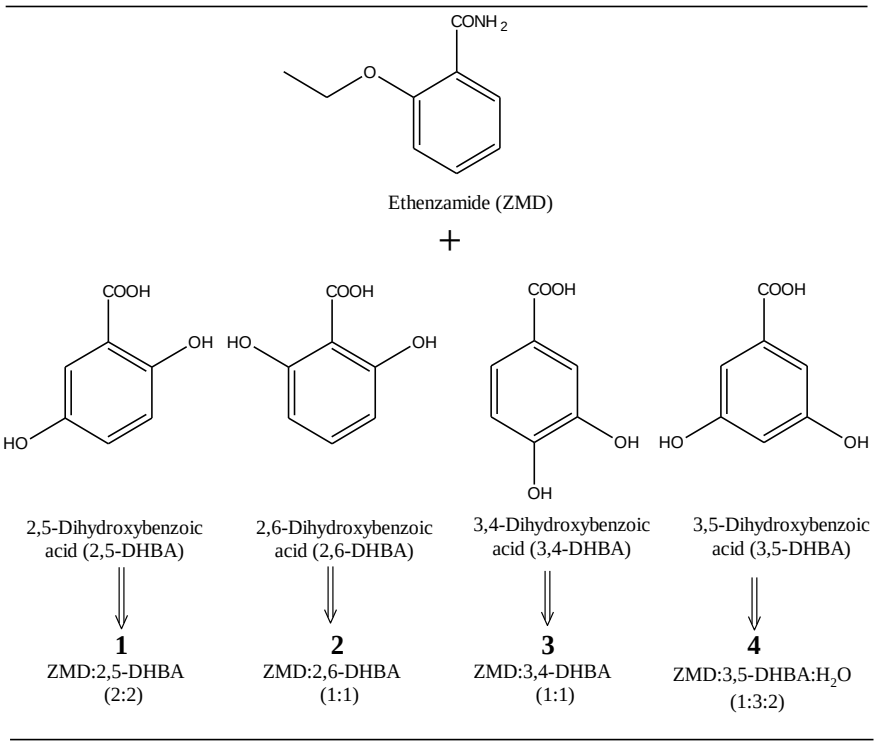

Scheme 4.1 Chemical structures of ethenzamide and isomeric dihydroxybenzoic acids used for cocrystallization and their stoichiometric ratio cocrystal formation.

Cocrystals are prepared to exploit different supramolecular interactions between drug···drug, drug···coformer and solute···solvent. These weak interactions essentially govern the drug physiochemical properties. The strength of supramolecular interactions that exists between drug and coformers have significant effects on different solute···solvents interactions, thereby modulates diffusion kinetics. The $CONH_2$···COOH hydrogen bonded heterosynthon is more favourable than COOH···COOH homosynthon in these cocrystals because of the stronger donor ($O-H_{COOH}$) and acceptor ($C=O_{CONH2}$) character. The *p*Ka values of $O-H_{COOH}$ [2.97 for 2,5-DHBA, 1.29 for 2,6-DHBA, 4.48 for 3,4-DHBA, and 4.04 for 3,5-DHBA] and p^{KHB} of acceptor $C=O_{CONH2}$ further suggested better bonding sites. Moreover, electrostatic surface potential charges at the acceptor sites (i.e. acceptor O of $C=O_{COOH}$ and $C=O_{CONH2}$) harmonizes the formation of a stable heterosynthon between the two functionalities. Also, the auxiliary hydrogen

bonding between $N-H_{CONH2}$ and $C=O_{COOH}$ contributed to the stability of the heterosynthon. This observation encouraged us to select isomers of dihydroxybenzoic acids for multicomponent solid formation. The presence of phenolic OH in the coformers was intentional to tune lipophilicity of the supramolecular aggregates.

4.3.2 Characterization of Cocrystals

The characteristic shifting of vibrational frequencies from the parent materials in FT-IR spectra indicates the formation of the cocrystals (Figure 4.1). The presence of hydrogen-bonded COOH group is assigned by the band at ~1700 cm^{-1} for C=O and the O−H group of the carboxylic acid at ~2500 cm^{-1}. The peak between 1690−1630 cm^{-1} assigned the stretching vibration of amide C=O. The appearance of stretching absorptions in between 3500−3100 cm^{-1} and the bending vibration in the range 1640−1550 cm^{-1} attributed the presence of hydrogen-bonded amide N−H.

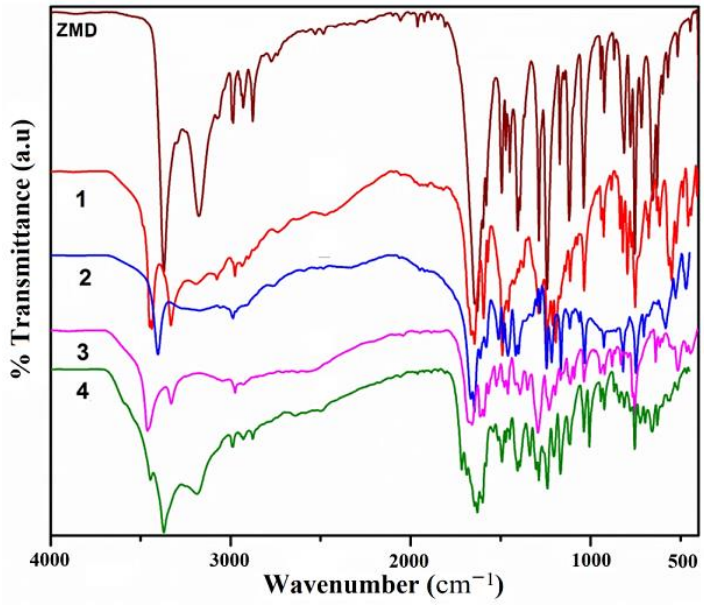

Figure 4.1 FT-IR spectra comparison of ZMD and its cocrystal **1** to **4.**

All the cocrystal materials exhibit single endothermic transitions on DSC which are measured by DSC (Figure 4.2, Table 4.1). The endotherm transition between 90−102 °C for **4** referred the loss of two water molecules, supported by TGA analysis (weight loss 5.4%) and Karl Fisher moisture micro analyser (water

content Calculated 5.4%, Experimental 5.3%). The release of two water molecules is also attributed to their presence in the single crystal lattice i.e. discussed later. All the cocrystals exhibit entirely different melting behaviour compared to their parent molecules indicating the purity of the cocrystal phases. The melting behaviour of the cocrystals and their parent molecules is depicted in Table 4.1

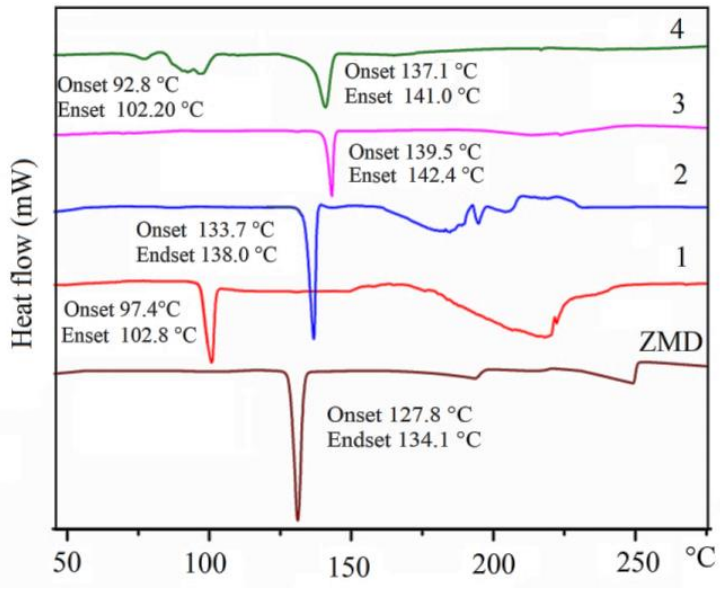

Figure 4.2 DSC endotherm plots of ZMD and its cocrystals **1** to **4**.

Table 4.1 Comparison of cocrystals melting parameters with melting of drug ethenzamide and their respective coformers.

Drug	Coformer	Coformer m. p. (°C)	Cocrystal	Solvent loss temperature (°C)		Cocrystals m. p. (°C)	
				Onset	Endset	Onset	Endset
ZMD [m. p.= 128-134]	2,5-DHBA	200-205	**1**	-	-	97.4	102.9
	2,6-DHBA	165	**2**	-	-	133.8	138.1
	3,4-DHBA	202-204	**3**	-	-	139.5	142.4
	3,5-DHBA	235-238	**4**	92.8	102.2	137.1	141.0

The formation of cocrystal is confirmed by PXRD analysis by comparing the PXRD patterns of cocrystal with their respective starting material. Moreover, the experimental powder X-ray patterns are compared with those simulated from the single-crystal structures which are discussed in the later section (Figure 4.3). Overlaid as well as Rietveld refinement showed the same peak positions and

patterns of intensities and exhibits good agreement with the simulated one which reassured the formation of single-phase material (Appendix Figure A.5) [20].

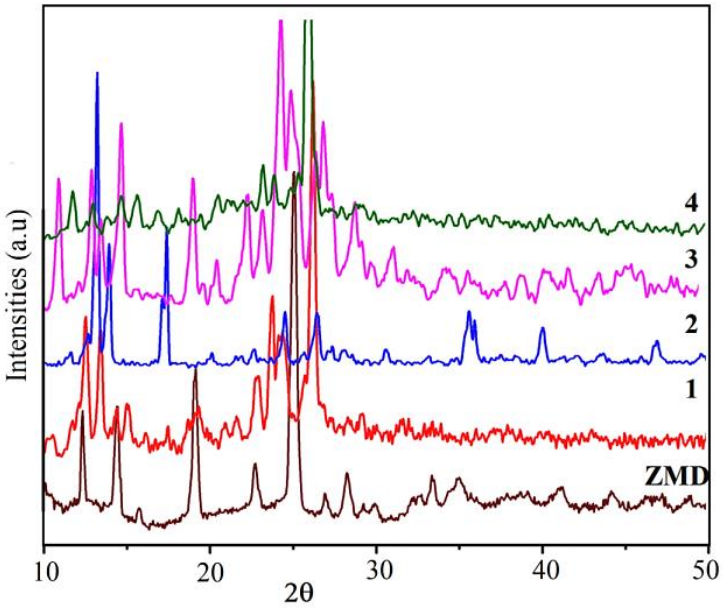

Figure 4.3 Stacked PXRD patterns of ZMD and its cocrystals **1** to **4**.

The single crystal structures of all four cocrystals are determined to understand the non-covalent interactions and molecular packing behaviour. The guest-free crystalline modification of **1**, **2**, and **3** was isolated in 1:1 stoichiometry, whereas **4** was detected as dihydrate (details are in experimental section). In crystal structure 1, the two symmetry independent molecules (one ZMD and one 2,5-DHBA) form acid···amide dimer heterosynthon via N–H···O and O–H···O hydrogen bonds (Figure 4.4a). These dimers are further connected by second symmetry independent 2,5-DHBA molecule eventually forming a zig-zag tap. Two such taps comprised a 2D molecular sheet that further stacked to each other via weak C–H···O and π···π interaction. The same acid···amide heterosynthon is also observed in the crystal structure of 2 and 4 (Figure 4.4b,d). Lack of free OH group in 2,6-DHBA constitute weak interactions such as C–H···O and π···π interactions that complete stacking of 2D molecular sheets. Unlike to structures 1 and 2, head-to-head acid···acid homo dimer between 3,4-DHBA via $R_2^2(8)$ supramolecular synthon is observed in 3 (Figure 4.4c). Remaining two OH groups connect these homodimers into a tape like structure via O–H···O interactions (2.16 Å, 142°) in

$R_2^2(10)$ motif. The ZMD molecule hangs on the O–H···O hydrogen bonded $R_2^2(10)$motif through N–H···O (2.13 Å, 174°) and O–H···O (2.16 Å, 142°) interactions.

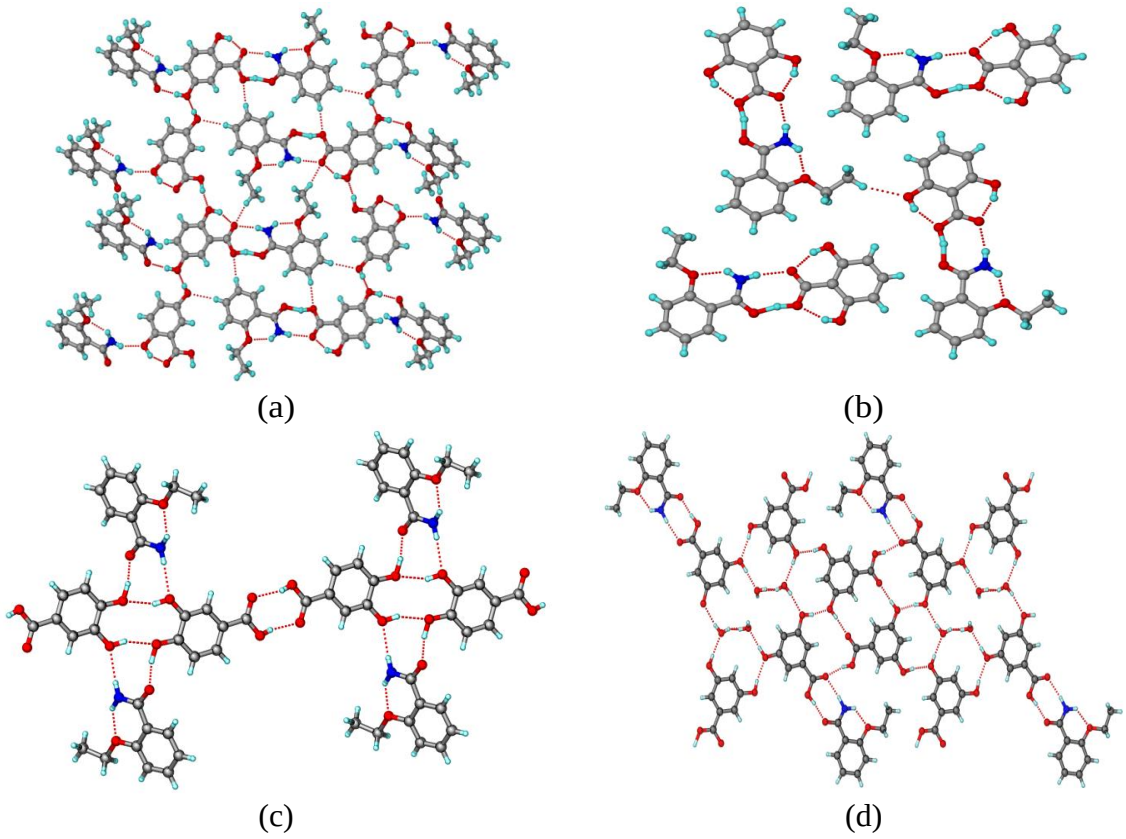

Figure 4.4 (a) Acid···amide heterosynthon via N−H···O and O−H···O hydrogen bonds in the crystal structure of **1**, (b) layer structure guided by weak C−H···O interaction in **2**, (c) acid···acid homosynthon in **3** and (d) layered crystal structure of **4** with acid···amide heterosynthon connected by water molecules.

The crystal structure of **4** was found dihydrate with one ZMD and three 3,5-DHBA in the asymmetric unit. Molecular arrangement showed a 2D layer structure with acid···acid homodimer and acid···amide heterodimer. The third asymmetric 3,5-DHBA did not participate in dimer formation, rather they along with water molecules connected homo and heterodimers via O–H···O hydrogen bonding.

Table 4.2 Hydrogen bond parameters in SCXRD of cocrystals **1** to **4**

Cocrystal	Interaction	H···A/Å	D···A/Å	∠D–H···A/ Å	Symmetry code
1	O_{11}–H_{2A}···O_7	1.46	2.505(13)	164	1-x,1-y,1-z
	N_1–H_{5A}···O_{19}	2.19	3.013(16)	156	1-x,1-y,-z
	N_2–H_{6A}···O_{10}	2.04	2.940(15)	167	1-x,1-y,1-z
	O_6–H_{8A}···O_9	1.80	2.753(14)	168	1+x,1+y,z
	O_{12}–H_{9A}···O_1	1.73	2.640(13)	172	1-x,1-y,-z
	O_{20}–H_{20A}···O_{12}	1.87	2.749(14)	178	-1+x,y,z
	C_{21}–H_{21}···O_{11}	2.45	3.368(18)	168	-1+x,-1+y,z
	C_{22}–H_{22}···O_{20}	2.48	3.384(18)	164	x,-1+y,z
	C_{26}–H_{26}···O_5	2.36	3.242(17)	157	-1+x,-1+y,z
2	N_1–H_{1B}···O_1	1.97	2.853(16)	167	–
	O_2–H_{2A}···O_5	1.35	2.439(14)	165	–
	C_{16}–H_{16B}···O_3	2.59	3.531(19)	161	x,-1+y,z
3	O_1–H_{1A}···O_2	1.88	2.612(3)	164	-x,-y,-z
	N_2–H_{2B}···O_3	2.13	2.971(4)	174	1-x,-y,-z
	O_3–H_{3A}···O_4	2.16	2.922(3)	142	1-x,1-y,-z
	O_4–H_{4A}···O_5	1.70	2.629(3)	152	x,1+y,z
4	N_1–H_{1A}···O_{10}	2.02	3.035(7)	169	1-x,1-y,-z
	O_1–H_{2A}···O_2	1.47	2.659(6)	168	-x,-y,-z
	O_3–H_{3A}···O_{15}	1.93	2.775(7)	167	1-x,1-y,1-z
	O_4–H_{4A}···O_{11}	1.97	2.822(6)	165	–
	O_6–H_{6A}···O_{10}	1.85	2.692(6)	160	-1+x,-1+y,1+z
	O_7–H_{7A}···O_5	1.88	2.709(6)	160	1-x,-y,2-z
	O_8–H_{8A}···O_3	1.81	2.764(7)	171	–
	O_9–H_{9A}···O_{12}	1.78	2.650(6)	168	1-x,1-y,-z
	O_{11}–H_{11A}···O_{16}	1.84	2.743(8)	171	1-x,1-y,1-z
	O_{14}–H_{14A}···O_7	1.74	2.691(7)	166	2-x,1-y,1-z
	O_{16}–H_{16B}···O_{15}	2.00	2.831(9)	172	–

4.3.3 Conformational Analysis of Ethenzamide Cocrystals

In general, transport properties of a material are understood in respects of the van der Waals interactions, structural arrangements and movements of molecules. Therefore, the solubility and permeation behaviour of a molecule in solution can be decided primarily by the packing of molecules and conformational cum steric effects existed by the short-range intermolecular forces. A Cambridge Structural

Database (ConQuest 1.18, build RC2, CSD version 5.37 May 2016 Updates, www.ccdc.cam.ac.uk) survey was performed to examine the conformational variation of ethenzamide molecules in the reported multicomponent systems of it. Interestingly, a significant change in the conformation of ZMD is noticed in all multicomponent crystals extracted from CSD (29 hits) and four cocrystals presented here.

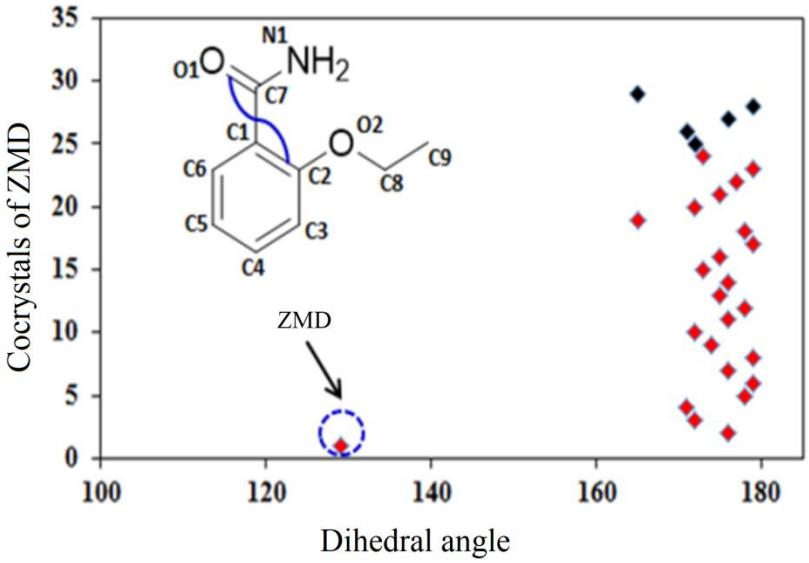

Figure 4.5 Dihedral angle of dangling amide group in pure ZMD and in ZMD cocrystals [circle – ZMD; red – CSD reported multicomponent systems; black – cocrystals **1** to **4**, present study].

The dihedral angle of dangling amide group in the single crystal structure of pure ZMD is 129° (Figure 4.5). While in all the reported cocrystal systems the angles are observed in the range of 170-179°. (Figure 4.5, CSD refcodes are presented in Appendix Table A.6). The cocrystals report publishing later this study also follows the same trend [21–23]. This increase in dihedral angle essentially contributed additional free energy to the conformation and thereby the newly adopted molecular planarity and symmetry of ZMD could provide a wider scope for solute···solvent interaction resulting in high solubility/permeation [3].

4.3.4 Phase Stability

Since the possibility of dissociation/phase transition of cocrystals or the hydrate formation of the drug during solubility and permeability experiments cannot be

ruled out, we performed stability test for of the cocrystal materials [24]. Accordingly, a slurry experiment for stability test in water is designed and performed (details in the experimental section 4.5.10). Sufficient amount of **3** was retrieved from the solution and recorded the PXRD pattern. We did not repeat these experiments for **2** and **4** as they were found stable by Karl Fisher titration experiment for water content measurement and thermogravimetric analysis. For comparison, a slurry experiment is performed for **1**. The PXRD pattern of the slurry of **1** retains the original peak position even after the experiment completes. This confirms the phase stability of **1**. Cocrystal **3** showed no significant change in PXRD pattern up to ~8h. But an additional peak at 2θ ~ 9.4 appeared after 8h and became prominent at 24h along with few other minor changes. The alteration in PXRD pattern with additional peak signified phase change, possibly the formation of a hydrate.

A similar experiment is carried out to check the stability of the materials (**1** to **4**) at pH 1.2 and 7.4 buffer solutions. An adequate amount of slurry was retrieved from the solution after 12 h and the PXRD pattern was recorded (Appendix Figure A.6**)**. The similarity of the peak pattern to that of the simulated pattern obtained from the single crystal XRD with some peak shifting confirmed the phase stability of the cocrystals. Alike the slurry in aqueous solution an additional peak at 2θ ~ 9.4 appeared in the PXRD pattern for the slurry of cocrystal **3** (Appendix Figure A.7**)**. However, cocrystal **4** is not stable up to 12 h as the PXRD pattern does not match the simulated pattern PXRD pattern; however, it resembles its anhydrous form (Figure 4.6).

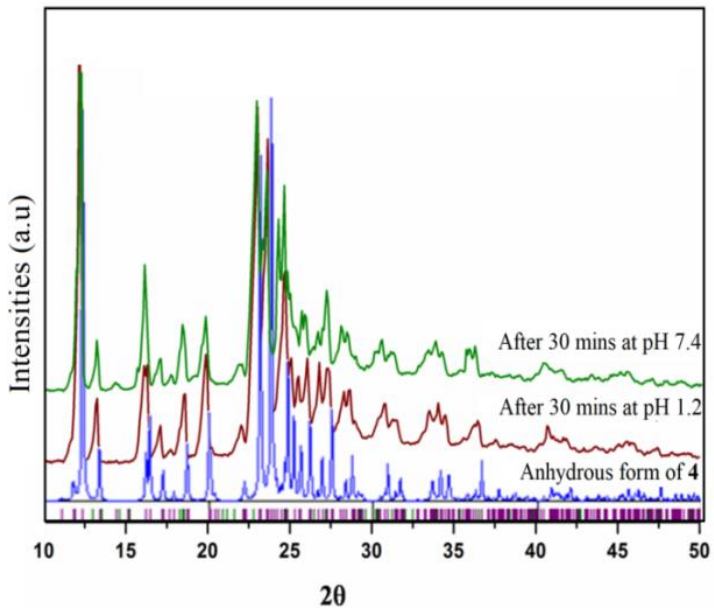

Figure 4.6 PXRD patterns of **4** upon slurry experiment revealing phase transformation to its anhydrous form.

4.3.5 Solubility in Different pH Buffers

The aqueous solubility of all four multicomponent materials (DHBA) and the parent drug (ZMD) is determined at ambient temperature. They exhibit improved solubility than ZMD, except cocrystal **1** shows marginal improvement. The observed solubility trend is **3** > **2** > **4** > **1** > ZMD (Figure. 4.7). While analysing the crystal structures we observe the existence of strong acid···amide heterosynthon and participation of free –OH group to form stronger hydrogen bonding to $C{=}O_{amide}$ in cocrystal **1.** This bonding plays a fair role in minimizing solute···solvent interactions, which indicates the lowering of aqueous solubility. Moreover, a close visualization of the crystal structure of **1** reveals that the stronger acid···amide dimer units are further linked via DHBA molecules to form interlocked molecular ladders. Whereas, the presence of weaker acid···acid homosynthon allowing two OH groups free for hydrogen bonding with polar solvents in **3** can be attributed to the better solubility. Nangia et al. demonstrated the phenomenon of lowering solubility of hydrated cocrystal based on the existing drug···water hydrogen bonding in the crystal lattice [14]. As a result, fewer sites remain available on the drug for solute···solvent interaction with water and consequently solubility decrease in the aqueous medium. Similar effects are

observed in **4**. The presence of two water molecules in the crystal lattice of **4** is attributed as the reason for its lower solubility but solubility enhanced gradually as the structure transformed into the anhydrous form.

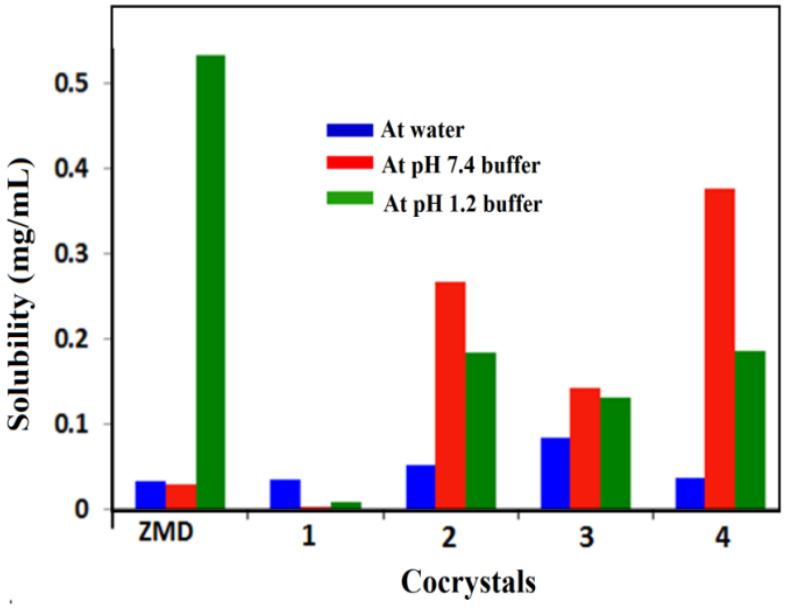

Figure 4.7 Solubility of cocrystals **1** to **4** and ZMD in pure water and at pH 1.2 & 7.4.

To understand the variation in the solubility behaviour, particle size distributions (PSD) are determined using a dynamic light scattering (DLS) method for at least three samples (details are in the experimental section). Cocrystals **1** and **3** are subjected to PSD studies and compared with ZMD. Interestingly, the particle size distribution of 1 is nearly identical (~0.8–4.0 micron) to that of ZMD (~0.7–3.5 micron). Similar PSD could contribute towards identical solubility behaviour of 1 and ZMD. However, the particle distribution for cocrystal 3 clearly indicates smaller particle size distributions (~0.001–0.005 micron) than ZMD, hence improved solubility.

The strength of the buffer composition can have a significant effect on the solubility/membrane permeation of a drug because of ionization of the drug over the pH range of the buffers used. The presence of micelles and monovalent (Na^+, Cl^- etc.) or trivalent (PO_4^{3-}) ions improves the solubilities and pharmacokinetic properties. These properties are also sensitive to the drug or coformers, which are

ionisable in the medium in which the parameters are determined. For example, at pH 7.4, donating a proton to the COOH group could make the coformer ionisable. These ions usually have surfactant properties, which promote better wetting of the drug-coformer particles and would explain the higher solubility rate. The solubility/membrane diffusion of cocrystal **1** is significantly lower than predicted at pH 1.2 and 7.4. The presence of Na^{+} and trivalent (PO_4^{3-}) ions in buffer could be a possible reason, which can form relatively insoluble complex coordinate with free phenolic OH group. A noteworthy increase in the solubility of ZMD than the cocrystals (**1** to **4**) at pH 1.2 has been observed. ZMD is known to form chloride salts at low pH and as a result, the tendency of protonated ZMD to interact with the solvent molecule increases, rendering its higher solubility. During the entire experiment, no significant change in pH of the solution is observed.

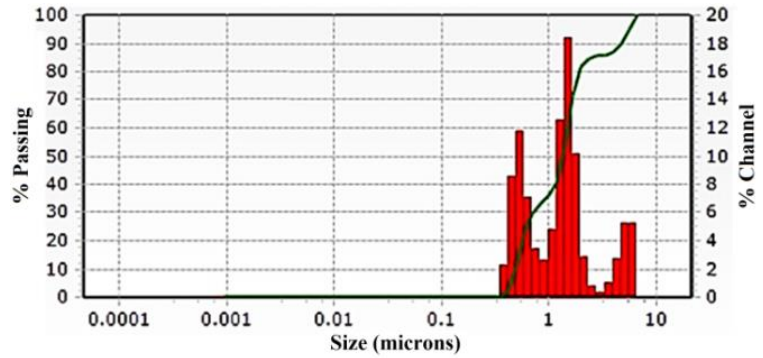

(a)

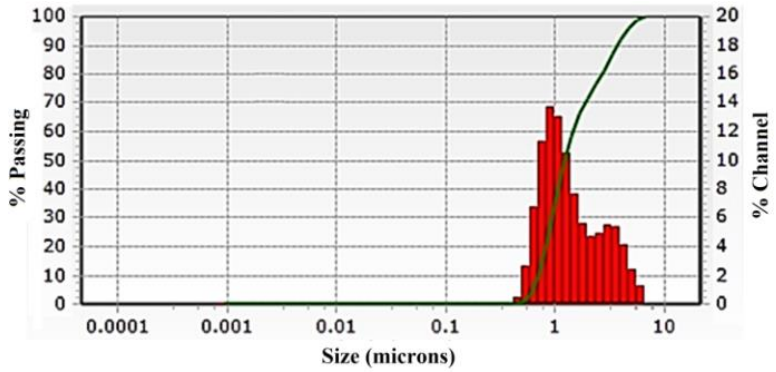

(b)

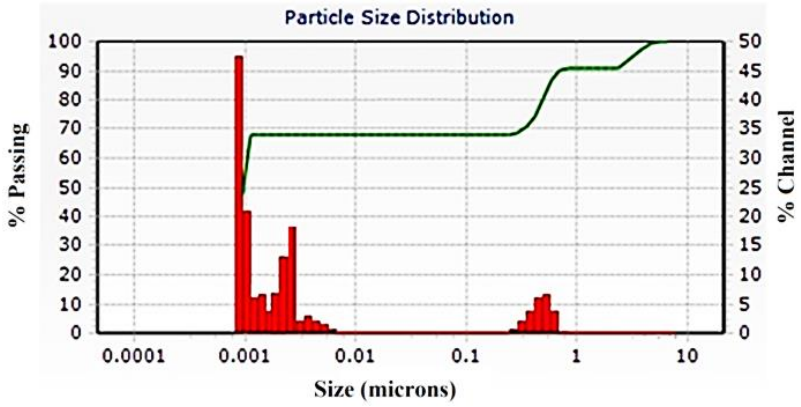

(c)

Figure 4.8 Particle Size Distribution plots for pure ZMD and cocrystal **1** and **3.**

4.3.6 Permeability

The membrane permeation behaviour of ZMD and its cocrystals **1** to **4** was measured (details in experimental section) at pH = 7.4 and pH = 1.2 and depicted in Figure 4.9. The value obtained and presented for the study is the average value calculated from three set of experiments. The cumulative amount of drug release with respect to time describes improved release kinetics and increases with time until it reaches the equilibrium. As expected, a maximum release was observed for cocrystal **2.** Whereas, cocrystal **4** releases slowly at pH 7.4 buffer [Phosphate Buffer Saline (PBS)]. The key factor for such change is the lipophilicity of the coformers and the interactions in the lattice. Lipophilicity of a compound is another important deciding factor for such properties exhibited by drug molecules which is measured by evaluating partition coefficient (log P). Generally, the log P value is a measure of lipophilicity or hydrophobicity when one of the solvents is water and the other is a non-polar solvent. Higher the log P value, higher is the lipophilicity, consequently higher is the thermodynamic activity [3,11]. The rise in membrane permeation of cocrystals in the order of **2** > **3** > **1** > **4** > ZMD at pH 7.4 can be attributed to the log P value of respective coformer [log P values: 2,6-DHBA (2.242); 3,4-DHBA (1.157); 2,5-DHBA (1.563); 3,5-DHBA (1.117)].

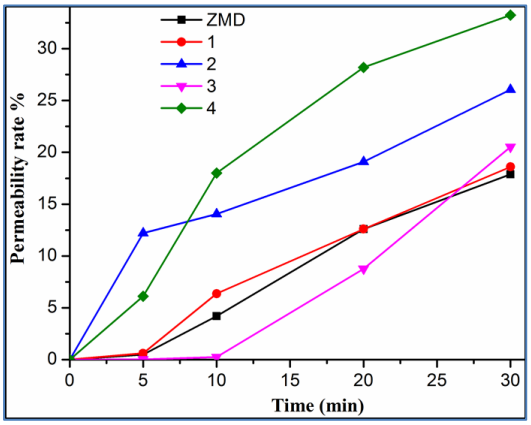

(a)

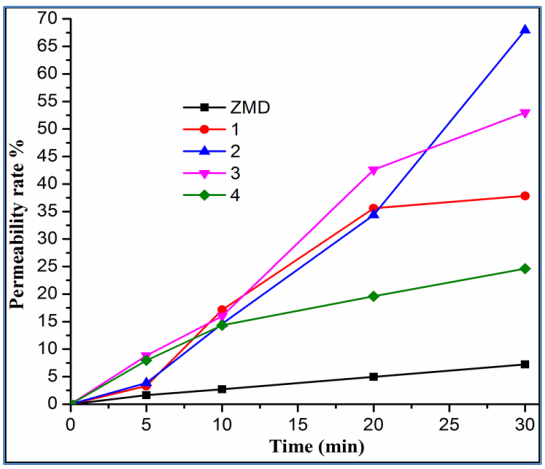

(b)

Figure 4.9 Permeability of multicomponent systems **1** to **4** and ZMD at (a) pH 1.2 and (b) pH 7.4

Quantitative calculation attributed the permeation behavior of 4 is better than the rest at pH 1.2 buffer solution. The pH 1.2 means the permeation of drug molecules must go across a highly acidic and ionic environment. Thus the presence of lattice waters in **4** might help in minimizing the interactions of cocrystal unit with the media and maximize the interaction of HCl with waters. The formation of ZMD hydrochloride salt at low pH has been known [25]. The curiosity of protonated ZMD to form short strong hydrogen bonds with the solvent molecule increases, rendering its higher solubility. These circumstances implied a rise in permeation in polar media. This eventually increases the flux of **1** to **4** and ZMD at initial 30

minutes and then gradually decreases with time. The flux calculation indicated high flux density for **2** and **3** at pH = 7.4 whereas at pH 1.2 it was **2** and 4 (Figure 4.10). The permeability rate % in pH 1.2 was also replicated at for each.

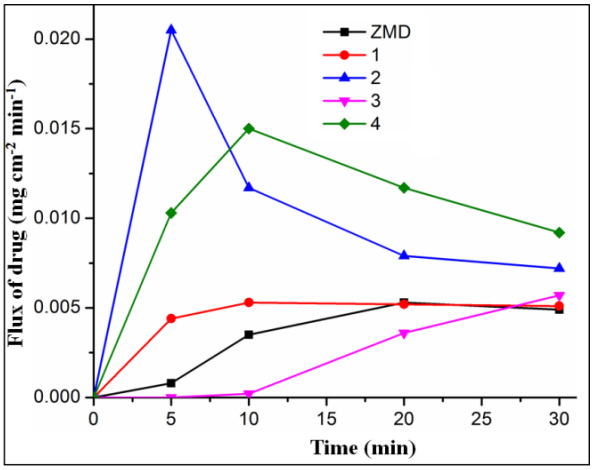

(a)

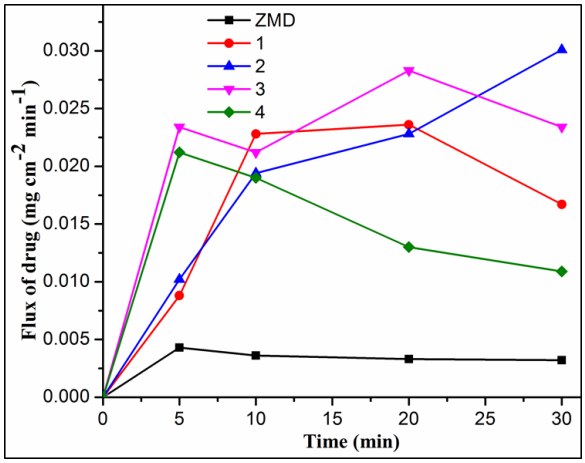

(b)

Figure 4.10 Flux of cocrystals **1** to **4** and ZMD at (a) pH 1.2 and (b) pH 7.4.

4.3.7 Hirshfeld analysis

To support the outcome from solubility and permeability experiments, Hirshfeld surface area analysis is performed for each cocrystal [26]. This analysis indicates the role of various interactions contribution and the molecular packing in the improvement of properties (Figure 4.11). The contribution of interaction percentage of polar O−H in cocrystals **1** (37%) and **4** (39%) are high when

compared with **2** (22%) and **3** (28%). Hence, the lesser interaction is accompanied by higher thermodynamic activity and eventually higher membrane permeability. In cocrystal **2** C−H interaction percentage is relatively high therefore making it more lipophilic. Consequently, the cocrystal unit move faster and permeation is high.

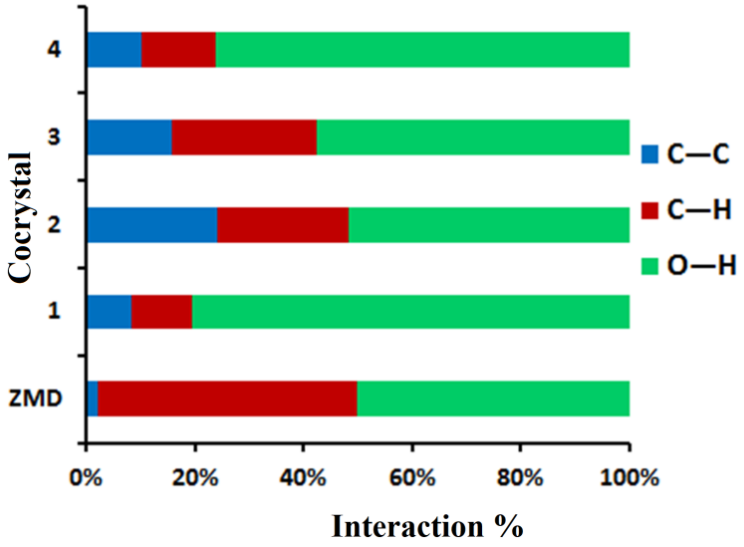

Figure 4.11 Percentage contribution of various weak interactions exists in ZMD and cocrystals **1** to **4** analysed by Hirshfeld surfaces.

4.4 Summary

The non-covalent interactions such as drug···coformer and solute···solvent interactions are crucial in cocrystal property modulation as they dictate the absorption, release and distribution of a drug in vitro. The study in this chapter emphasizes the correlation exists between non-covalent interactions and effective bioavailability. Four cocrystals of BCS class-II drug ethenzamide with dihydroxybenzoic acids are synthesized and characterized. Solubility and diffusion kinetics of these cocrystals have been determined at different pH buffers. Conformational twist of drug ethenzamide has been investigated for the reported cocrystals and examined the correlation of properties with molecular symmetries. Though the difference in property is not so drastic I present drug cocrystal system, several extremely important parameters that can significantly influence drug bioavailability/ efficacy have been probed in this study and anticipated an important message for drug formulation department.

4.5 Experimental Section

4.5.1 Materials

Drug ethenzamide (purity ≥ 99%) was purchased from Sigma-Aldrich and isomeric dihydroxybenzoic acids from Alfa Aesar. The analytical grade solvents used for the studies were obtained from Merck and used without further purification. Millipore water was used to carry out solubility and diffusion/permeability experiments.

4.5.2 Preparation of Cocrystals

A mixture of ethenzamide (ZMD) and a conformer in 1:1 molar ratio were taken in a mortar and pestle. The mixture was grinded for 30-40 minutes via liquid assisted grinding technique by dropwise addition of CH_3CN. The powder mixture was further dissolved in common laboratory solvents such as methanol, ethanol, etc. and kept for crystallization at room temperature. The cocrystals obtained after slow evaporation of solvent within 2-3 days (Scheme 4.1). Details are depicted in Table 4.3. All materials are characterized using thermal analysis, spectroscopy and X-ray diffraction techniques.

Table 4.3 Synthesis of ZMD multicomponent systems with dihydroxybenzoic acid coformers

Drug	Coformer	Crystallization solvent	Cocrystal	Stoichiometry/ solvent
Ethenzamide	2,5-DHBA	Toluene + Ethyl acetate	**1**	2:2
	2,6-DHBA	Methanol	**2**	1:1
	3,4-DHBA	Toluene + Acetonitrile	**3**	1:1
	3,5-DHBA	Methanol + Chloroform	**4**	1:3/ 2 H_2O

4.5.3 Vibrational Analysis

The IR spectra of ZMD and its multicomponent systems were recorded separately in Perkin Elmer Spectrophotometer using the KBr pellets ranging from 450 to 4000 cm^{-1} (Figure 4.1). Cocrystal formation was easily figured out by comparing the shifting of vibrational frequencies of the functional groups such as N−H, C=O

and C−O stretching frequency of ZMD that participated in hydrogen bonding with coformers.

4.5.4 Differential Scanning Calorimetry (DSC)

DSC endotherms of ZMD and cocrystal materials were recorded on a Mettler Toledo DSC 822e module in the range of 50−300 °C at 5 °C min^{-1} scan rate. Prior to the experiment, the instrument was calibrated for temperature and heat flow accuracy using the melting of pure indium (mp 156.6 °C and ΔH of 25.45 J/g). Single melting temperature onset confirms the formation of single-phase multicomponent solids (Figure 4.2, Table 4.1).

4.5.5 Thermogravimetric Analysis (TGA)

The DSC endotherm responsible for solvent release within 90─110 °C for 4 was reconfirmed by the TGA scans, which was recorded on a Shimadzu 60 model. The experiment was carried out at a heating rate of 10 °C min^{-1} under a nitrogen flow of 50 mL min^{-1}.

4.5.6 Powder X-ray Diffraction

Powder XRD of all samples including ZMD was recorded on a Bruker D8 Focus X-Ray Diffractometer, Germany using Cu-Kα X-radiation (λ = 1.54056 Å) at 35 kV and 25 mA. Diffraction patterns were collected at a scan rate of 5° min^{-1} (Figure 4.3). Rietveld refinement was performed for phase purity using Powder Cell 2.3.

4.5.7 Single crystal X-ray Diffraction

Single crystal X-ray diffractions were collected on a Bruker SMART APEX-II CCD diffractometer using Mo Kα (λ =0.71073 Å) radiation [27]. Bruker SAINT software has been employed for reducing the data and SADABS for correcting the intensities of absorption [28]. All cocrystal structures were solved and refined using SHELXL with anisotropic displacement parameters for non-H atoms [29]. In all crystal structures, H-atoms are located experimentally, whereas C–H atoms were fixed geometrically using the HFIX command in SHELX-TL [29]. The

figures and packing diagrams are made using X-Seed [30]. No any missed symmetry observed in the final check of the CIF file using PLATON [31]. Information of crystallographic parameters for all structures is furnished in Appendix Table A.5. The hydrogen bond distances in the X-ray crystal structures (Table 4.2) are neutron-normalized by fixing the D–H distance to its accurate neutron value (O–H 0.983 Å, N–H 1.009 Å, C–H 1.083 Å). The formation of various supramolecular hydrogen-bonded synthons in the cocrystals is presented in Figure 4.4.

4.5.8 Particle Size Distribution (PSD)

The particle size distribution (PSD) was determined using a dynamic light scattering (DLS) method utilising Nanotrac Wave II zeta potential analyser. The sample was grinded into a fine powder using a mortar and pestle for 30 min. The powdered sample was dispersed in media using sonication

4.5.9 Hirshfeld Surface

Crystal explorer 3.0 has been employed to generate the Hirshfeld molecular surfaces of each cocrystal materials. The various percentages of intermolecular interactions among the elements in the crystals are depicted (Figure 4.11), whereas the unique 2D fingerprint plots generated using *di* and *de* pair of coordinates. .

4.5.10 Phase Stability

An adequate amount of multicomponent crystalline material was taken for slurry experiments in order to examine the phase stability of materials during the experiments. Each experiment was performed in a jacketed, circulating flask maintained at 25 °C and in 3 sets to assure consistency. Needed amount of slurry of each material was retrieved at the time interval of 8h, 12h and 24h and recorded its PXRD pattern.

4.5.11 Solubility

The solubility of each material synthesized and ethenzamide was determined using Agilent Cary-60 double beam UV-Visible spectrophotometer at room temperature

for two different pH i.e. pH 7.4 and 1.2. The solubility parameter was calculated using the formula C_u = (A_u–intercept)/Slope, where C_u and A_u being the concentration and absorbance of the unknown solution. An excess amount of drug (ZMD) and its cocrystal (1 to 4) was added to 3 ml of the buffer at ambient temperature in a jacketed water vessel connected to a circulating water bath. The mixture was stirred at a rate of 80 rpm. We maintained the temperature of syringes, pipettes, filters, vials and needles utilized in experiments by preheating at the same temperature in an oven. The solubility observed after 12 h are an average of at least two determinations. The solubilities quoted were further correlated with that obtained from gravimetric measurements. A third set of experiment was also performed for solubility determination in pure water.

4.5.12 Permeability

Permeability experiment of the API and the synthesized four cocrystals was performed in a diffusion apparatus using cellulose membrane (MW 14000, Himedia, India) following the reported procedure by Desiraju et al. [12] Diffusion behavior was studied at buffer solution with two different pH (i.e. 1.2 and 7.4). Prior to this experiment, the membrane was treated along with 2% $NaHCO_3$ for 30 min at 80 °C to remove the trace amount of sulphides, followed by treatment with 10 mM of EDTA under constant conditions to get rid of any heavy metals and eventually with deionized water to remove glycerine from the membrane. The treated membrane was then mounted in clips and placed in diffusion cells. Dialysis membrane acting as donor compartment was placed with the suspension of ZMD and its cocrystal materials. The drug and/or cocrystal solution was then allowed to stir at about 80 rpm (at 25 °C), followed by diffusion through the membrane towards the receptor compartment filled with 150 mL phosphate-buffered saline (pH = 7.4). A similar procedure was followed for permeation at a solution with pH 1.2. Amount of substance released towards the receptor compartment through the dialysis membrane was further analysed by UV-Vis spectrophotometer. As such about 3 mL of the sample was taken out from the receptor compartment at a definite interval of time and added an equal volume of solution to maintain the volume constant. During the process, we could not observe any significant change in the pH of the buffered solution at the receptor compartment.

4.6 References

[1] Amidon, G. L., Lennernäs, H., Shah, V. P., and Crison, J. R. A theoretical basis for a biopharmaceutic drug classification: the correlation of in vitro drug product dissolution and in vivo bioavailability. *Pharmaceutical research*, 12(3):413-420, 1995.

[2] Dahan, A., Miller, J. M., and Amidon, G. L. Prediction of solubility and permeability class membership: provisional BCS classification of the world's top oral drugs. *The AAPS Journal*, 11(4):740-746, 2009.

[3] Ishikawa, M. and Hashimoto, Y. Improvement in aqueous solubility in small molecule drug discovery programs by disruption of molecular planarity and symmetry. *Journal of Medicinal Chemistry*, 54(6):1539-1554, 2011.

[4] Miller, J. M., Beig, A., Carr, R. A., Spence, J. K., and Dahan, A. A win-win solution in oral delivery of lipophilic drugs: Supersaturation via amorphous solid dispersions increases apparent solubility without sacrifice of intestinal membrane permeability. *Molecular Pharmaceutics*, 9(7):2009-2016, 2012.

[5] Trask, A. V. An overview of pharmaceutical cocrystals as intellectual property. *Molecular Pharmaceutics*, 4(3):301-309, 2007.

[6] Weyna, D. R., Cheney, M. L., Shan, N., Hanna, M., Zaworotko, M. J., Sava, V., Song, S., and Sanchez-Ramos, J. R. Improving Solubility and Pharmacokinetics of Meloxicam via Multiple-Component Crystal Formation. *Molecular Pharmaceutics*, 9(7):2094-2102, 2012.

[7] Thakuria, R., Delori, A., Jones, W., Lipert, M. P., Roy, L., and Rodríguez-Hornedo, N. Pharmaceutical cocrystals and poorly soluble drugs. *International Journal of Pharmaceutics*, 453(1):101-125, 2013.

[8] Steed, J. W. The role of co-crystals in pharmaceutical design. *Trends in Pharmacological Sciences*, 34(3):185-193, 2013.

[9] Qiao, N., Li, M., Schlindwein, W., Malek, N., Davies, A., and Trappitt, G.

Pharmaceutical cocrystals: An overview. *International Journal of Pharmaceutics*, 419(1-2):1-11, 2011.

[10] Sanphui, P., Devi, V. K., Clara, D., Malviya, N., Ganguly, S., and Desiraju, G. R. Cocrystals of hydrochlorothiazide: Solubility and diffusion/permeability enhancements through drug-coformer interactions. *Molecular Pharmaceutics*, 12(5):1615-1622, 2015.

[11] Yan, Y., Chen, J. M., and Lu, T. B. Simultaneously enhancing the solubility and permeability of acyclovir by crystal engineering approach. *CrystEngComm*, 15(33):6457-6460, 2013.

[12] Gopi, S. P., Ganguly, S., and Desiraju, G. R. A Drug-Drug Salt Hydrate of Norfloxacin and Sulfathiazole: Enhancement of in Vitro Biological Properties via Improved Physicochemical Properties. *Molecular Pharmaceutics*, 13(10):3590-3594, 2016.

[13] Jung, M. S., Kim, J. S., Kim, M. S., Alhalaweh, A., Cho, W., Hwang, S. J. and Velaga, S. P. Bioavailability of indomethacin-saccharin cocrystals. *Journal of Pharmacy and Pharmacology*, 62(11):1560-1568, 2010.

[14] Babu, N. J. and Nangia, A. Solubility Advantage of Amorphous Drugs and Pharmaceutical Cocrystals. *Crystal Growth & Design*, 11(7):2662-2679, 2011.

[15] Khatioda, R., Saikia, B., Das, P. J., and Sarma, B. Solubility and: In vitro drug permeation behavior of ethenzamide cocrystals regulated in physiological pH environments. *CrystEngComm*, 19(46):6992-7000, 2017.

[16] Pekoe, G., Van Dyke, K., Mengoli, H., Peden, D., and English, D. Comparison of the effects of antioxidant non-steroidal anti-inflammatory drugs against myeloperoxidase and hypochlorous acid luminol-enhanced chemiluminescence. *Agents and actions*, 12(1-2):232-238, 1982.

[17] Aitipamula, S., Chow, P. S., and Tan, R. B. H. Trimorphs of a pharmaceutical cocrystal involving two active pharmaceutical ingredients: Potential relevance to

combination drugs. *CrystEngComm*, 11(9):1823-1827, 2009.

[18] Przybyłek, M., Ziółkowska, D., Mroczyńska, K., and Cysewski, P. Propensity of salicylamide and ethenzamide cocrystallization with aromatic carboxylic acids. *European Journal of Pharmaceutical Sciences*, 85:132-140, 2016.

[19] Sarmah, K. K., Boro, K., Arhangelskis, M., and Thakuria, R. Crystal structure landscape of ethenzamide: a physicochemical property study. *CrystEngComm*, 19(5):826-833, 2017.

[20] Rietveld, H. M. A profile refinement method for nuclear and magnetic structures. *Journal of Applied Crystallography*, 2(2):65-71, 1969.

[21] Khatioda, R., Bora, P., and Sarma, B. Trimorphic Ethenzamide Cocrystal: In Vitro Solubility and Membrane Efflux Studies. *Crystal Growth & Design*, 18(8):4637-4645, 2018.

[22] Nechipadappu, S. K. and Trivedi, D. R. Cocrystal of nutraceutical sinapic acid with Active Pharmaceutical Ingredients ethenzamide and 2-chloro-4-Nitrobenzoic acid: Equilibrium solubility and stability study. *Journal of Molecular Structure*, 1171:898-905, 2018.

[23] Sokal, A., Pindelska, E., Szeleszczuk, L., and Kolodziejski, W. Pharmaceutical properties of two ethenzamide-gentisic acid cocrystal polymorphs: Drug release profiles, spectroscopic studies and theoretical calculations. *International Journal of Pharmaceutics*, 522(1-2):80-89, 2017.

[24] Bethune, S. J., Huang, N., Jayasankar, A., and Rodríguez-Hornedo, N. Understanding and Predicting the Effect of Cocrystal Components and pH on Cocrystal Solubility. *Crystal Growth & Design*, 9(9):3976-3988, 2009.

[25] Perumalla, S. R. and Sun, C. C. Synthon preference in O-protonated amide crystals-dominance of short strong hydrogen bonds. *CrystEngComm*, 15(44):8941-8946, 2013.

[26] Spackman, M. A. and Jayatilaka, D. Hirshfeld surface analysis. *CrystEngComm*,

11(1):19-32, 2009.

[27] *BRUKER AXS (v 6.14); Bruker AXS Inc.: Madison, WI*. 2008.

[28] *SAINT Plus, Bruker AXS Inc.: Madison, WI*. 2008.

[29] Sheldrick, G. M. *SHELXS97 and SHELXL97: Programs for Crystal Structure Solution and Refinement University of Göttingen*. 1997.

[30] Spek, A. L. *PLATON, A Multipurpose Crystallographic Tool Utrecht University, Utrecht, Netherland*. 2002.

[31] Spek, A. L. and IUCr Single-crystal structure validation with the program *PLATON*. *Journal of Applied Crystallography*, 36(1):7-13, 2003.